Polymer Testing 109 (2022) 107545

Contents lists available at ScienceDirect

Polymer Testing

journal homepage: www.elsevier.com/locate/polytest

Fused Filament Fabrication 3D printed polypropylene/ alumina nanocomposites: Effect of filler loading on the mechanical reinforcement

Nectarios Vidakis [a,b], Markos Petousis [a,b,*], Emanuel Velidakis [a,b], Nikolaos Mountakis [a,b], Peder Erik Fischer-Griffiths [c], Sotirios A. Grammatikos [c,**], Lazaros Tzounis [a,b,d,***]

[a] Mechanical Engineering Department, Hellenic Mediterranean University, Estavromenos, 71004, Heraklion, Crete, Greece
[b] Institute of Emerging Technologies (i-EMERGE) of HMU Research Center, Heraklion, 71410, Crete, Greece
[c] Laboratory of Advanced & Sustainable Engineering Materials (ASEMlab), Department of Manufacturing & Civil Engineering, NTNU-Norwegian University of Science and Technology, Building B', Teknologivegen 22, 2815, Gjøvik, Norway
[d] Department of Materials Science and Engineering, University of Ioannina, Ioannina, 45110, Greece

ARTICLE INFO

Keywords:
Fused filament fabrication (FFF)
Three-dimensional (3D) printing
Polypropylene (PP)
Aluminum oxide (Al_2O_3)
Nanocomposites

ABSTRACT

Three-dimensional (3D) printed Polypropylene (PP) reinforced with aluminum oxide (Al_2O_3) nanoparticles (NPs) were developed and fully characterized in this study. Nanocomposite filaments were produced initially following a melt mixing extrusion process, utillised as feedstock for the Fused Filament Fabrication (FFF) specimen manufacturing. Al_2O_3 NPs at 0.5, 1.0, 2.0 and 4.0 wt% loadings were melt-mixed with the PP thermoplastic matrix. Specific geometry samples were 3D printed and analysed via tensile, flexural, viscoelastic, impact, microhardness and fractographic investigations. Raman spectroscopy verified the polymeric structure and the incorporated Al_2O_3 NPs within the polymer matrix. Atomic Force Microscopy (AFM) of the extruded filaments revealed the nanoscale roughness induced by the alumina nanoinclusions. All 3D printed nanocomposite structures exhibited enhanced tensile, flexural and thermomechanical properties. Specifically, the best combination was found for the 1.0 wt% loaded specimen showing a tensile and flexural strength increase by approx. 4% and 19%, respectively, with a concomitant slight increase in impact and microhardness properties compared to unfilled PP. Dynamic Mechanical Analysis (DMA) revealed a stiffening mechanism for the PP/Al_2O_3 nanocomposites being in good agreement with the quasi-static mechanical tests. It could be envisaged that the 3D printed PP/Al_2O_3 nanocomposites developed herein could find numerous applications as engineered thermoplastics, where enhanced material's static and dynamic mechanical properties are required.

1. Introduction

Additive Manufacturing (AM) has gained a significant scientific and industrial interest over the last decades in various sectors ranging from advanced fiber reinforced polymer (FRP) composites [1], construction and buildings [2], up to the fabrications of printed photovoltaics [3], biomedical equipment [4] and scaffolds for tissue engineering [5]. The manufacturing of components and end-use products with customisable geometries could be easily realised via AM, especially when small batches are required, implausible for conventional manufacturing processes that present several limitations and freedom to fabricate parts with complex shapes [6].

Three-dimensional (3D) printing is the flagship amongst AM technologies and it has been in the forefront of research during the last years, as well as continuously gaining more maturity for industrial applications replacing conventional manufacturing technologies i.e. injection moulding, computer numerical control (CNC) machining, plastic forming (PF), and (plastic) joining [7]. Relatively, 3D printing can be realised directly from computer-aided design (CAD) models, which can be more complex compared to conventionally machined parts, increasing thus the design freedom, as well as enabling mass customization allowing the reduction of the post-production assembly steps [8]. From the ever

* Corresponding author. Mechanical Engineering Department, Hellenic Mediterranean University, Estavromenos, 71004, Heraklion, Crete, Greece.
** Corresponding author. Laboratory of Advanced & Sustainable Engineering Materials (ASEMlab), Department of Manufacturing & Civil Engineering, NTNU-Norwegian University of Science and Technology, Building B', Teknologivegen 22, 2815, Gjøvik, Norway.
*** Corresponding author. Mechanical Engineering Department, Hellenic Mediterranean University, Estavromenos, 71004, Heraklion, Crete, Greece.
E-mail addresses: markospetousis@hmu.gr (M. Petousis), sotirios.grammatikos@ntnu.no (S.A. Grammatikos), tzounis@hmu.gr (L. Tzounis).

https://doi.org/10.1016/j.polymertesting.2022.107545
Received 8 May 2021; Received in revised form 3 December 2021; Accepted 10 March 2022
Available online 12 March 2022

increasing number of 3D printing processes, the most well-known and widely employed ones are the: *i)* Selective Laser Sintering (SLS), *ii)* Stereolithography, *iii)* Fused Filament Fabrication (FFF), *iv)* Material Jetting and Drop on Demand (DOD), *v)* Binder Jetting, and *vi)* Digital Light processing (DLP) [9].

Fused Filament Fabrication (FFF) is known as one of the most promising 3D printing technologies among others, especially when it comes to versatility, scalability and cost i.e. both feedstock material cost and 3D printer machinery cost, all of which have rendered the FFF 3D printing applicable both for home applications, as well as for various advanced and industrial applications [10]. Typically, thermoplastic polymeric materials in the form of a filament are used as the feedstock, being heated above their melting point (T_m) and extruded with a movable nozzle in the X–Y direction to generate a 3D structure in a layer-by-layer manner [11]. As such, FFF has numerous advantages and could offer a direct solution to: *i)* the acute shortage of goods, as for instance in the actual COVID-19 pandemic situation [12], *ii)* freedom of design of 3D objects, *iii)* mass customization, and *iv)* reduced material's consumption leading to waste minimization [10].

Although there has been great achievements regarding the FFF printers' automation and accuracy, all affecting the 3D printed part quality and the final 3D printed object properties, FFF is limited currently by the availability of functional thermoplastic materials, with most of the existing stock filament materials being reported in literature so far [13–15]. Relatively, the physicochemical properties i.e. electrical, thermal, magnetic, etc. of the feedstock filament material could endow multi-functional properties to the 3D printed objects, giving an added value to the potential final end-product [16]. Moreover, the filament melt rheological properties may be tuned via additives well-known as viscosity modifiers, polymer blends, nanoparticulate additives, etc. resulting into high quality printed parts, high production yield and production rate FFF printing based processes [17].

To date, there is an increasing demand for FFF 3D printable materials exhibiting multifunctional properties; i.e. combined physical with enhanced mechanical properties [6]. Namely, functional and novel thermoplastic materials as filaments i.e, electrically conductive [18], thermoelectrically enabled [19], magnetically active [20], capacitive and piezoresistive [21], flexible and stretchable [22], mechanically reinforced [23], antimicrobial [24], etc. have been used for FFF 3D printing yielding 3D objects with on-demand properties. Polymer nanocomposites could offer thus a unique approach towards novel filaments and FFF 3D printed derived objects. To that end, one has to consider the nanoparticle filler geometry, density, surface chemistry, as well as nanoscale interactions e.g. the well-known filler-filler interaction and filler-matrix interactions that have profound implications on the macroscopic behavior of the 3D printed nanocomposite objects, the quality of the printing process, etc. [25].

Polypropylene (PP) belongs to the group of polyolefin thermoplastic materials, while amongst other polyolefins i.e. HDPE, LDPE, PE and PS, polypropylene is semicrystalline in nature and the most widely used one, due to its exceptional mechanical properties i.e. high mechanical strength, as well as low cost, processability and excellent chemical stability [26]. PP mechanical, as well as thermomechanical properties are significantly affected by the manufacturing process and more specifically to the plausible shear induced crystallization as suggested by the relevant literature [27]. The crystallization of PP causes thermal shrinkage phenomena upon cooling of the melt, thus making 3D printing more challenging, as it affects the bonding between adjacent filament strands and layering interfusion, as well as the adhesion of the deposited layers on to the build plate [28]. However, PP inherent properties in combination with its market price, could promote it as a fundamental material for FFF 3D printing processes. Therefore, thorough instigations are necessary to elucidate the process-structure-property relationship and possible mechanical property improvements i.e. by the addition of nanoparticulate inclusions.

A great number of studies on polypropylene nanocomposites have been reported so far, both regarding isotactic (i-PP) and syndiotactic PP (s-PP), with considerable improvements of polypropylene's thermal stability [27], electrical conductivity [29], crystallization behavior [30], and mechanical properties [31]. Namely, PP/organoclay nanocomposites for FFF 3D printing have been developed with a significant enhancement in the storage modulus for the nanocomposites with the highest clay filler loading at 15% (enhancements have been shown also for the 5% and 10%) [32]. Aumnate et al. recently reported on reinforcing polypropylene with graphene-polylactic acid microcapsules for FFF 3D printed objects. Specifically, at very low graphene loading (0.75 wt%), the 3D printed construct showed neither shrinkage nor warping, while graphene nanocomposite 3D printed constructs with 30% volume fraction infill exhibited higher mechanical performance compared to the neat PP [33]. In another study related to 3D printed isotactic polypropylene/graphene nanocomposites, the authors reported that the presence of graphene induced shear thinning during extrusion, while at 5% and 10% of graphene loading, the storage modulus decreased considerably; namely nearly 50% for the 10% loading [34]. Recently, Lei et al. reported on FFF 3D printed carbon black (CB)/polypropylene nanocomposites with excellent microwave absorption performance [35], while Kwok et al. reported on PP/CB electrically conductive nanocomposite filaments for FFF 3D-printed circuits and sensors [36], both focusing only onto the electrical properties of the 3D printed nanocomposites. Aluminum oxide (Al_2O_3) nanoparticles (NPs) exhibit a great number of functional properties, such as being an electrical insulator, optical transmission, extremely chemically inert and stable at high temperatures, while it is a commonly used mineral additive in composite industry and already reported as nanoadditive improving the mechanical properties of PP nanocomposites [30]. To the best of the authors' knowledge, there is no existing literature reporting on the utilization of Al_2O_3 NPs as nanofillers and their effect on the mechanical reinforcement of 3D printed PP specimens.

In the study at hand, the focus is given on studying the effect of spherical Al_2O_3 NPs with ~50 nm size, on various concentrations, in PP 3D printed structures. Melt mixing and 3D printing, both have the advantage to be complete solvent-free and cost-efficient methods for fabricating high-quality PP/Al_2O_3 nanocomposites and bulk parts respectively, thus both can be directly implemented at industrial 3D printing manufacturing scale. The 3D printed nanocomposites were investigated by Scanning Electron Microscopy (SEM) regarding their microstructure via fractured surfaces, as well as for their surface morphology as a means to elaborate the layers' fusion quality. Atomic Force Microscopy (AFM) revealed that the extruded filaments' surface roughness increases in general with the increased Al_2O_3 NP filler loading. Raman spectroscopy proved the nanocomposite spectroscopic responses, owing to the PP and Al_2O_3 NP characteristic fingerprints. Detailed mechanical investigations i.e., tensile, flexural, impact, microhardness, and Dynamic Mechanical Analysis (DMA) revealed the structure-property relationship of the fabricated 3D printed nanocomposite materials, as well as elucidating the mechanical reinforcement mechanisms under static and dynamic mechanical loadings for the PP/Al_2O_3 nanocomposites with different filler loadings.

2. Experimental section

2.1. Materials

Polypropylene (PP) in powder form was used throughout this study as the polymer matrix procured by Hellenic Petroleum S.A. (Athens, Greece), under the trademark of Ecolen PP (powder form). Ecolen PP type is an isotactic homopolymer PP (i-PP) utilized in a wide range of engineering applications, while its Melt Volume-Flow Rate (MVR) was calculated to be ~34 cm^3/10 min, according to ISO 1133:2005. Aluminum oxide (Al_2O_3) spherical nanoparticles (NPs) were purchased from Sigma Aldrich (St. Louis, MO, USA) with an average particle diameter of ~50 nm.

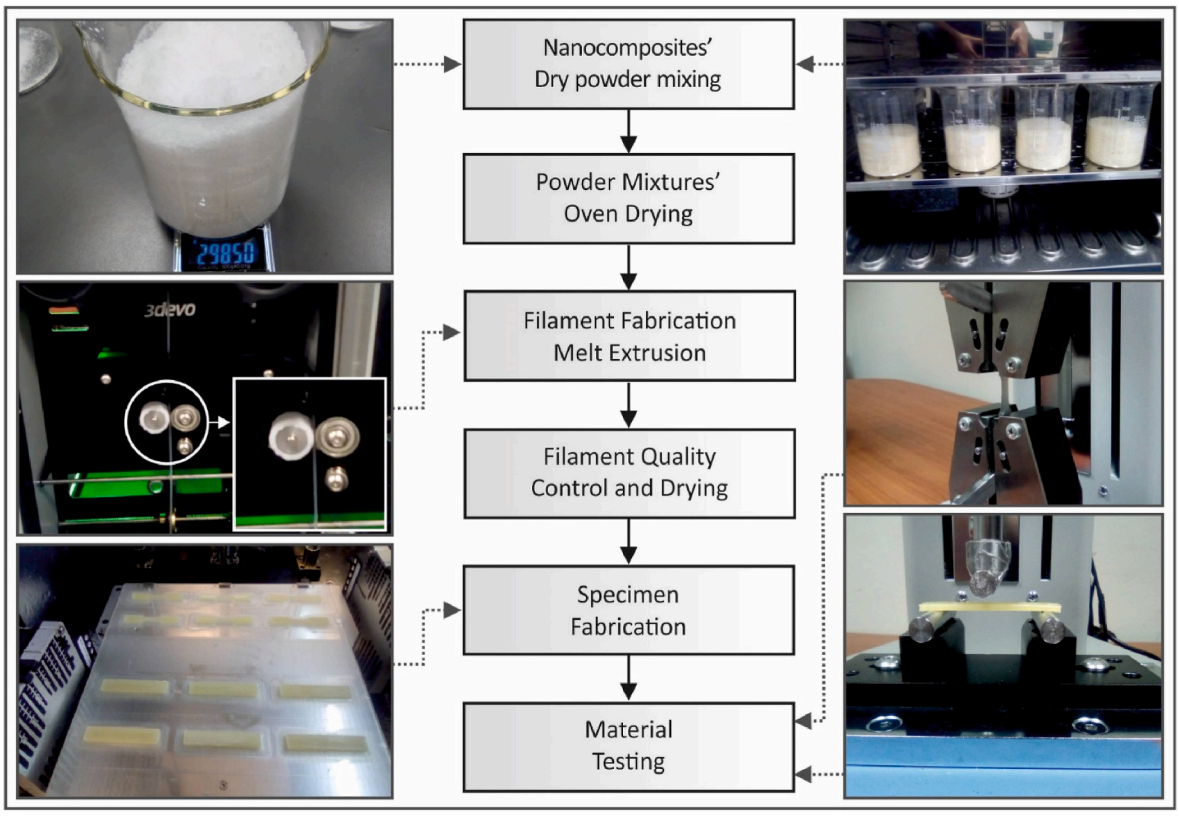

Fig. 1. Flow chart illustrating the different steps to manufacture the filaments, as well as the 3D printed specimens (neat PP and PP/Al_2O_3 nanocomposites).

2.2. *Filament fabrication and FFF 3D printing process parameters for PP and PP/Al_2O_3 nanocomposites*

PP was physically mixed initially with Al_2O_3 NPs using a mechanical homogenizer at different filler concentrations (0.5, 1.0, 2.0 and 4.0 wt %). The mixture was dried prior to the extrusion process for the FFF 3D printing nanocomposite filaments' production (predetermined quantities for each filament extrusion batch). Hereafter the PP/Al_2O_3 nanocomposites, either the extruded filaments or the 3D printed specimens, are denoted as PP/Al_2O_3 (0.5 wt%), PP/Al_2O_3 (1.0 wt%), PP/Al_2O_3 (2.0 wt%) and PP/Al_2O_3 (4.0 wt%) for the 0.5, 1.0, 2.0 and 4.0 wt% filler loadings, respectively. Neat PP and nanocomposite PP/Al_2O_3 powder mixtures were dried in an oven at 80 °C overnight before the filament extrusion process.

For the filament extrusion, a 3D Evo Composer 450 single screw extruder (3d evo B.V., NL) preheated at 350 °C, was used. This extruder has a specially designed screw for mixing materials and additives, according to the extruder's vendor. Extruder's temperatures were set to 195 °C for the first heat zone, 210 °C for heat zones two (2) and three (3) and 205 °C at the final fourth (4th) heat zone before the nozzle. Extruder's rotational speed was set to 3.5 rpm and an extra air duct was used to achieve a smooth cooling procedure and finally high-quality roundness of the filament. A built-in sensor in the extruder was continuously measuring the produced filament diameter micro-adjusting the extruding speed, to maintain a constant and precise diameter of the produced filament. The optimum melt mixing and filament extrusion process parameters for neat PP and PP/inorganic NP nanocomposite filaments have been determined in our previous study [31]. The extrusion process yielded in all cases 1.68 mm ± 0.07 mm in diameter filaments, which is adequate accuracy for consistent 3D printing and a typical diameter FFF 3D printing. Quality control inspection of the filament was conducted before each 3D printing process, as well as filament drying at 80 °C overnight. The filament diameter was inserted in the slicer program to calculate the necessary feed rate that

Parameters	Value	Units
Printing orientation	45	Deg.
Layer thickness	0.200	mm
Bed temperature	90	°C
Nozzle temperature	255	°C
Number of perimeters	2	
Top solid layers	4	
Bottom solid layers	4	
Fill Density	100	%
Travel speed	30	mm/s

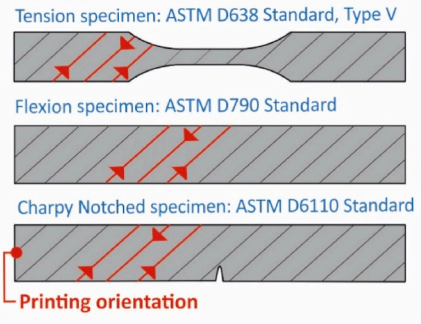

Fig. 2. The optimum FFF 3D printing parameters followed in this study and set up to slicer software in order to manufacture the neat PP as well as the PP/Al_2O_3 different nanocomposite specimens.

should be automatically used during the whole 3D printing process. Fused Filament Fabrication (FFF) was selected to manufacture the neat PP as well as the PP/Al_2O_3 nanocomposite specimens using a Intamsys Funmat HT 3D FFF technology 3D Printer (Intamsys Technology Co. Ltd., Shanghai, China). Initial trials were performed to obtain the optimum FFF 3D printing parameters (set of parameters), giving high quality of 3D printing process for the PP and the PP/Al_2O_3 nanocomposite systems in this study. The specimens were built with the following 3D printing parameters: 100% solid infill, 45° deposition orientation angle, 0.2 mm layer height and 255 °C 3D printing nozzle temperature. To avoid applying 3D printing adhesive aids (such as 3D printing glues), as well as to save the building specimens from warping or detaching from the heated print bed, it was concluded that is essential to maintain a sealed shut 3D printing area, in order to maintain constant temperature in the 3D printing chamber. For the mechanical characterisation investigations, all 3D models for the 3D printing have been designed using the 3D design Autodesk® Fusion 360™ (Autodesk®, Inc.) software, while being finally exported to Standard Tessellation Language (STL) files.

Fig. 1 illustrates schematically the methodology flow chart followed to produce the neat PP, as well as the PP/Al_2O_3 nanocomposites used for the different measurements. Fig. 2 summarizes the 3D printing parameters employed for the manufacturing of the specimens with different geometries required for the different mechanical tests carried. All specimens were 3D printed in the horizontal direction.

2.3. Characterization techniques

Raman spectroscopy was performed for the pure PP, as well as the PP/Al_2O_3 nanocomposite 3D printed specimens, using a Labram HR-Horiba (Kyoto Japan) scientific micro-Raman system. An optical microscope equipped with a 50 × long working distance objective was utilized for delivering the excitation light and collecting the back-scattering Raman activity. An Ar^+ ion laser line (514.5 nm) at 1.5 mW power at the focal plane (this power corresponds to the focal plane with a laser spot diameter of ~3 μm) was utilized for the Raman excitation.

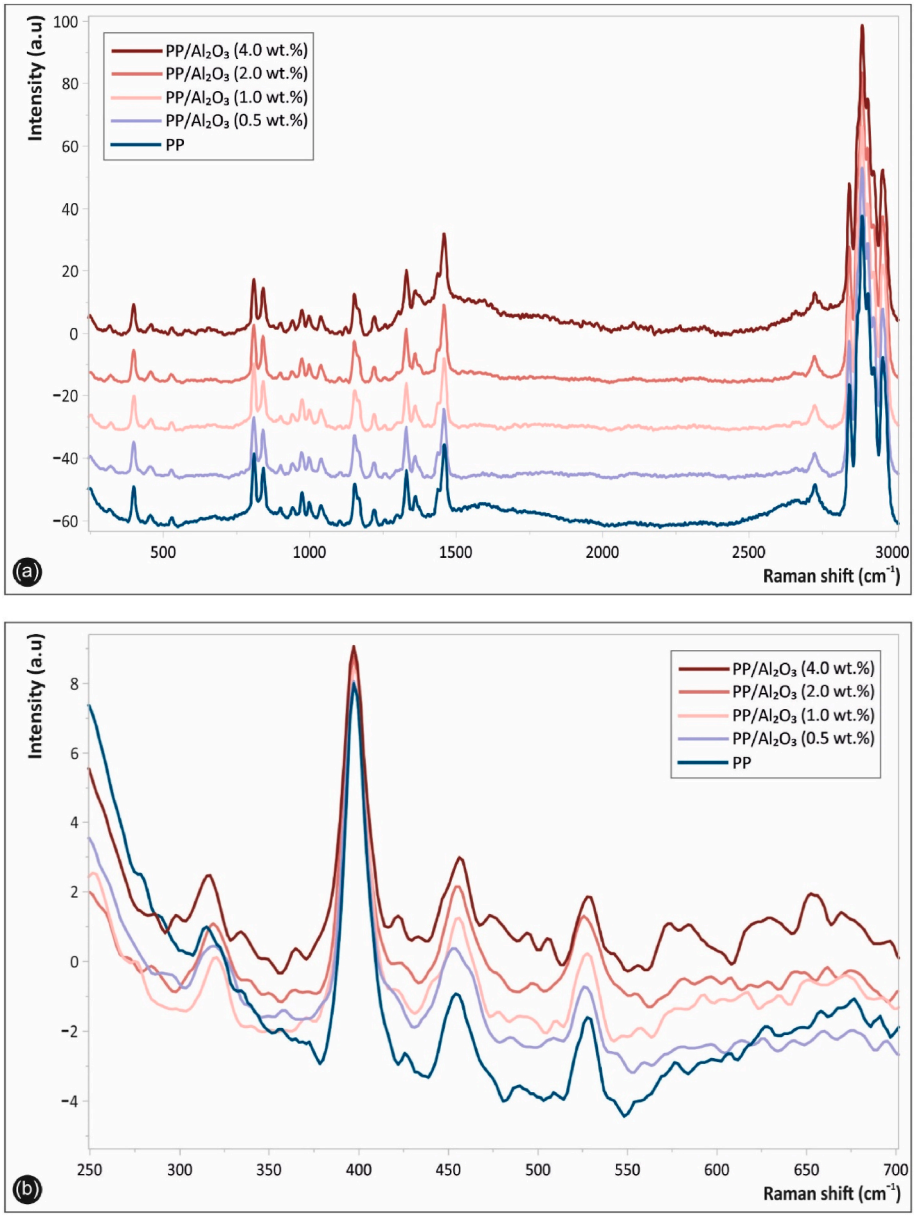

Fig. 3. Raman spectra of 3D printed samples, namely the pure PP, as well as the PP/Al_2O_3 nanocomposites at different filler loadings, in the spectral region of (a) 250–3000 cm^{-1}, and (b) 250–700 cm^{-1}, respectively.

All acquired spectra shown in this work have been treated with a baseline correction through subtraction of a linear or polynomial fit of the baseline from the raw spectra, to remove tilted baseline variation caused by various noises, i.e., fluorescent background, etc.

The flow properties of PP and PP/Al_2O_3 nanocomposites were tested using an Instron CEAST MF20 Melt Flow Tester (UK). Tests were conducted following the ASTM D1238-10 (Standard Test Method for Melt Flow Rates of Thermoplastics by Extrusion Plastometer) for all samples. The basic principle of the method involves i) the thermal heating of the granulated thermoplastic to molten state, and ii) its forced flow out of a capillary die. An extruding piston is used that is loaded with dead weights, up to 21.6 kg. In this work, 4 min pre-conditioning (in the chamber) without any weight was employed, using dead weights of 2.16 kg.

SEM characterization was used to analyze the nano/micro structuring of both the 3D printed specimens' side surface, as well as the fractured surfaces of 3D printed tensile specimens. SEM microstructural analyses have been performed using a JEOL JSM 6362LV (Jeol Ltd., Massachusetts, USA) electron microscope in high-vacuum mode at 5 kV acceleration voltage. Prior to SEM investigations, samples were sputter coated with a 5 nm Au thin film to avoid charging effects. Additionally, this device was used for Energy Dispersive X-Ray Analysis (EDs) on uncoated samples (specimens and Al_2O_3 nanoparticles powder), to verify the materials in the nanocomposites.

Atomic Force Microscopy in Tapping Mode (TM-AFM) was performed with a scanning probe microscope (MicroscopeSolver P47H Pro, NT-MDT Moscow Russia) in air at room temperature (23 °C) at a resonant frequency of 300 kHz. Commercially available silicon cantilevers were used with scanning frequency of 1 Hz, a tip cone angle of 20°, a cantilever spring constant of 35 N/m and tip radius of about 10 nm. Extruded filament roughness values were determined after 2nd flattening operation over the captured area of 5 × 5 μm^2 height images using the Nova RC-1 NT-MDT image analysis software.

Quasi-static tensile test experiments were carried out at room temperature (23 °C) following the ASTM D638-02a. According to the standard, a type V specimen of 3.2 mm thickness was chosen, and a total of six (6) specimens were manufactured and tested for each case. An Imada MX2 (Imada inc., Northbrook, Illinois, USA) tension/flexure test apparatus in tensile mode using standardized grips was utilized to carry out the tensile test experiments at an elongation rate of 10 mm/min.

Flexural (three-point bending) tests were carried out also at room temperature conditions on 3D printed specimens (64.0 mm length, 12.4 mm width, and 3.2 mm thickness), according to the ASTM D790-10 (three-point bending test with 52.0 mm support span). Flexural test specimens were also manufactured with the same 3D printing parameters as for the tensile test specimens. An Imada MX2 machine in flexural mode setup was employed for the three-point bending tests. The same speed of 10 mm/min was set for the testing procedure, and a total of six (6) specimens were manufactured and tested for the neat as well as PP/Al_2O_3 nanocomposites.

Impact tests were performed according to the ASTM D6110-04. Specimens were 3D printed with the following dimensions: 80.0 mm (length) × 8.0 mm (width) × 10.0 mm (thickness). Six (6) specimens in total were tested using a Terco MT 220 (Terco, Sweden) Charpy's impact apparatus. Release height of the apparatus hammer was the same for all the experiments.

Microhardness measurements were conducted according to the ASTM E384-17. The specimens' surface was fully polished before each set of measurements. An Innova Test 300- Vickers (Innovatest Europe BV, Maastricht, NL) apparatus was employed, while the applied force was set to 100 gF and duration of 10s was selected for indentation. Imprints were measured under six (6) different specimens for each one of the PP and PP/Al_2O_3 nanocomposites.

Dynamic Mechanical Analysis (DMA) was performed using a TA Instruments DMA850 instrument (Denmark). Samples were 3D printed in dimensions of: length 58.0–60.0 mm, width 14.0–15.0 mm, and thickness 2.7–3.2 mm. Due to the samples having rough side edges from the FFF manufacturing process, all samples were polished in two steps using 240 and 400 grain sandpaper under water flow. Prior to testing, samples were dried at a temperature of 35 °C for a minimum of 48 h. The DMA testing procedure consisted of a temperature ramp from room temperature to 130 °C (and in some cases up to 135 °C), at a rate of 3 °C min^{-1}. Testing was conducted using the 3-point bending fixture. Samples were preloaded to 0.1 N. A sinusoidal displacement was applied to the samples with a constant amplitude of 30.0 μm and a frequency of 1.0 Hz throughout the tests. Data was collected by the instrument at a sampling rate of 0.33 Hz. The recorded parameters were the storage modulus, loss modulus, tan δ, temperature, time, and oscillation angular frequency.

3. Results and discussion

3.1. Raman analysis of neat PP and PP/Al_2O_3 nanocomposites

Raman spectroscopy provides valuable information regarding the associated vibrations of lattice ions in the unit cell (i.e. optical phonons at the centre of the Brillouin zone) in the case of crystals, whereas vibrational, rotational and other low frequency modes of molecules in a system within the irradiated scattering volume [37]. Among the various polymorphs of Al_2O_3, γ-Al_2O_3 and η-Al_2O_3 do not exhibit any significant bands in the Raman spectrum. In this study, it is envisaged that the Al_2O_3 NPs is a mixture of various crystallinity polymorphs of Al_2O_3. Specifically, Fig. 3 shows the Raman spectra of the respective 3D printed samples, namely the pure PP, as well as the PP/Al_2O_3 nanocomposites at different filler loadings. Fig. 3a shows the whole acquired Raman spectrum in the range of 250–3000 cm^{-1}, while Fig. 3b the 250–700 cm^{-1} spectral region. All peaks attributed to the PP matrix macromolecular chains' chemistry i.e., due to the polymer chain backbone and the side groups, are depicted with continuous lines in Fig. 3a, while the specific bands assigned to Al_2O_3 NPs are illustrated with dashed lines in

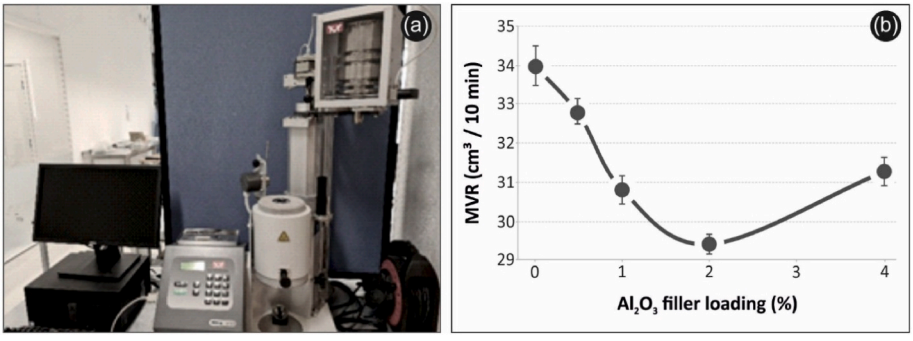

Fig. 4. (a) Melt flow measurements experimental setup, (b) Average MVR values for the neat PP and the PP/Al_2O_3 nanocomposite at different filler loadings, along with their deviations.

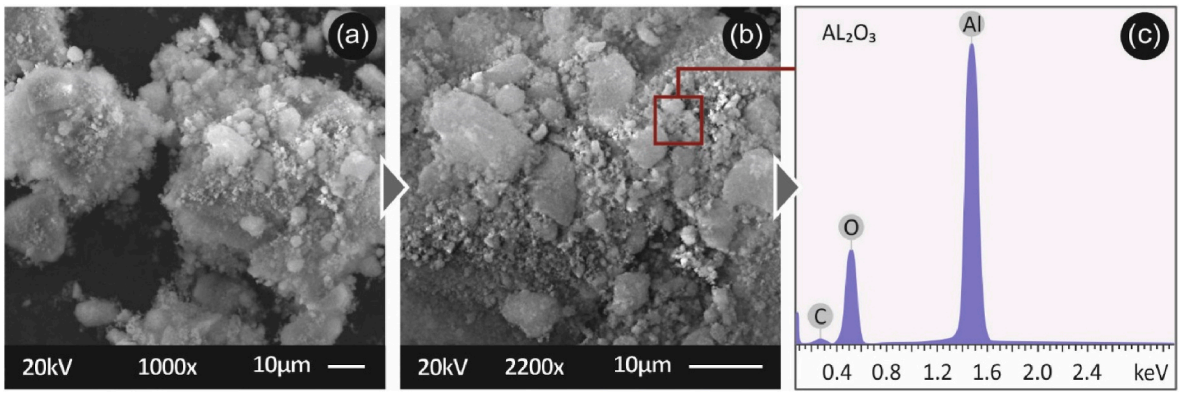

Fig. 5. SEM images of the Al_2O_3 powder at two magnifications (a) 1000x, (b) 2200x and (c) the corresponding EDS graph of the Al_2O_3 powder.

Fig. 3b. For all nanocomposites, the characteristic PP peaks can be seen as have been reported elsewhere [31]. The characteristic fingerprints of PP are located at ca. 385, 810, 868, 967, 1036, 1168 and 1221 cm^{-1} (C–C stretching vibration), 1250 and 1320 cm^{-1} (CH deformation vibration), 1334 and 1454 cm^{-1} (–CH_2 of the PP backbone macromolecular chains), 1361–1385 cm^{-1} (–CH_3 deformation vibrations of PP chains, as well as the –CH_3 side group rocking vibration) [38], and 2721, 2837, 2875 and 2962 cm^{-1} (CH_3 symmetric and asymmetric stretching vibration) [39]. The spectra of PP/Al_2O_3 nanocomposites at the different Al_2O_3 wt.% filler loading exhibit some additional peaks attributed to the incorporated Al_2O_3 nanocrystalline NP vibrational modes, indicated more clearly in Fig. 3b. Namely, peaks at ca. 368 cm^{-1}, 423 cm^{-1}, 432 cm^{-1}, 575 cm^{-1} and 633 cm^{-1} correspond to vibrational modes of Al_2O_3 NPs with different crystallinities i.e., α-Al_2O_3, γ-Al_2O_3 and η-Al_2O_3. being in good agreement with the typical alumina nanoparticulate vibrational modes reported elsewhere, while the band at ~575 cm^{-1} could be assigned to the Al_2O_3 degenerate class of vibrations [40]. It is worth mentioning and it can be observed that the corresponding Al_2O_3 peaks' intensity is slightly increasing with the increased filler loading for the different nanocomposites. Moreover, alumina peaks are already observed for the PP/Al_2O_3 (0.5 wt%) lowest filler loading nanocomposite specimens, indirectly verifying a sufficient and high level of nanoparticles' dispersion within the polymeric matrix.

3.2. Melt flow volume index (MVR) of neat PP and PP/Al_2O_3 nanocomposites

The MVR, alternative to the well-known melt-flow index (MFI) has been determined in this study (Fig. 4) for the neat PP and the PP/Al_2O_3 nanocomposites. The MVR could more precisely elaborate the thermoplastic materials' processability, as well as indicate any unexpected and plausible melt processing problems may be encountered during the molten state layer-by-layer material's deposition, otherwise known as 3D filamentous extrusion printing. The MVR reflects in other words the ease of flow of a thermoplastic polymer in melt state, providing thus a quality control index, which is quite important especially for the FFF 3D printing manufacturing method.

Fig. 4a shows the experimental setup for the MVR measurements. Five specimens were tested from each material and Fig. 4b shows the average MVR measured values, along with their deviation. As it can be observed in Fig. 4, the MVR value exhibited a slight decrease from ~34.0 cm^3/10min for the neat PP to ~32.8 cm^3/10min for the PP/Al_2O_3 (0.5 wt%), whilst for the case of 1.0 wt% and 2.0 wt% filler loadings MVR value showed a significant drop to ~30.9 and ~29.4 cm^3/10min, respectively. This drop was expected, as the filler content increases the viscosity of the polymer melt. The PP/Al_2O_3 (4.0 wt%) nanocomposite unexpectedly showed some less viscous behavior (MVR increases to

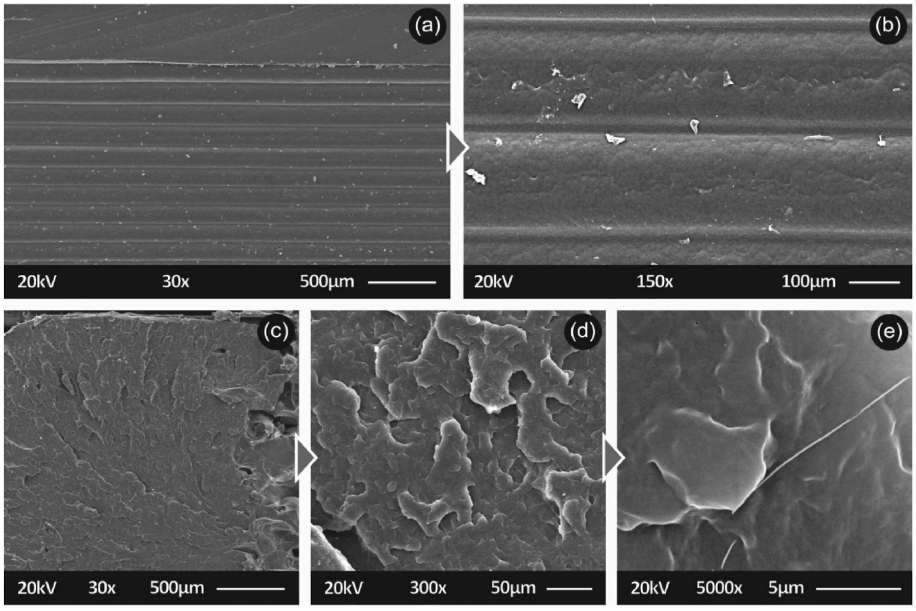

Fig. 6. SEM images of the pure PP 3D printed tensile specimens (a) side surface at 30x, (b) side surface at 150x, (c) fracture surface at 30x, (d) fracture surface at 300x, (d) fracture surface at 5000x

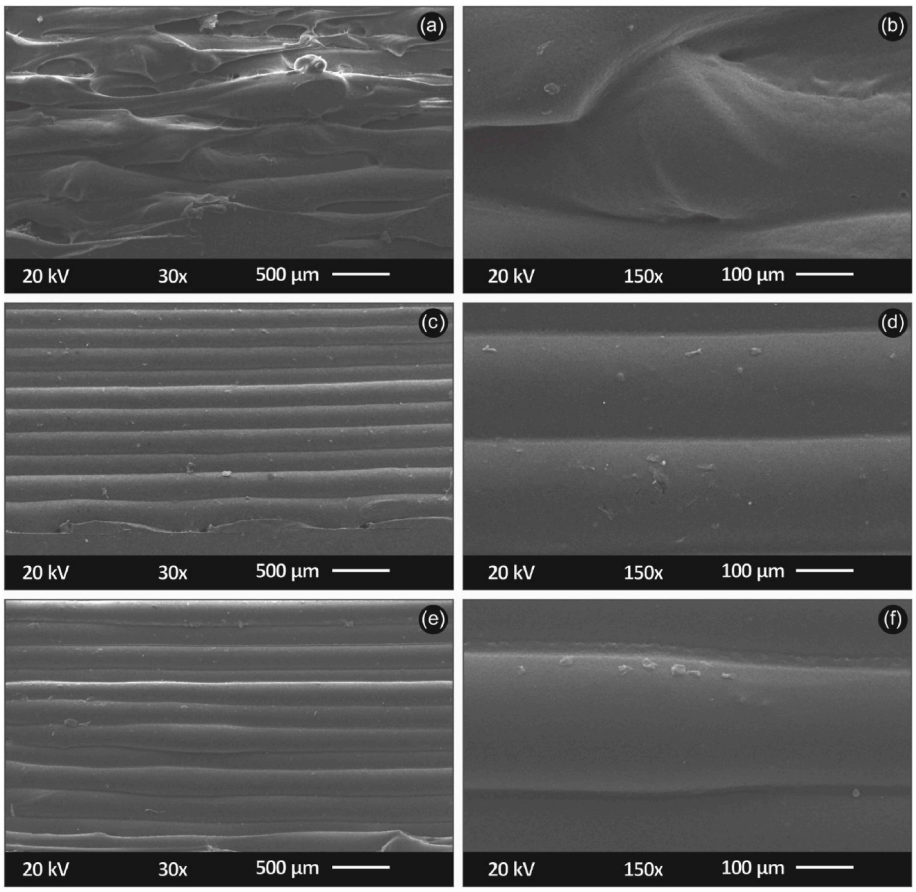

Fig. 7. Side surface morphology of PP/Al_2O_3 3D printed nanocomposites at two different magnifications: (a, b) PP/Al_2O_3 (0.5 wt%), (c, d) PP/Al_2O_3 (2.0 wt%), and (e, f) PP/Al_2O_3 (4.0 wt%).

~31.2 cm^3/10min), which is possibly attributed to some nanoparticle micro-agglomerate formation that tend to disturb the nanodispersion achieved up to the 2 wt% filler loading, due to inherent nanoparticle van der Waals forces' interactions and/or possible electro-hydrodynamic and electro-osmotic effects [41].

3.3. SEM microstructure

In Fig. 5 SEM images of the Al_2O_3 powder are shown, along with the corresponding EDS graph of the Al_2O^3 powder. The nanostructure of the filler's powder is clearly shown (Fig. 5a and b), while any microscale structures are attributed to the deposition of the powder in the carbon tape for the observation in the SEM apparatus. In the EDS analysis, the Al peak dominates the graph, as expected, verifying the existence of the Al material in the filler (Fig. 5c). Fig. 6 shows SEM images from pure PP 3D printed tensile specimens. The side surface images (Fig. 6a and b) show an excellent build structure and fusion between the layers. The images from the fracture surface (Fig. 6c, d, 6e) show a rather ductile failure on the specimen.

The 3D printed specimens' external structure and interlayer fusion has been characterised through SEM microstructural analysis of the 3D printed samples' side surface morphology (at two different magnifications). Fig. 7 depicts the side surface morphologies of 3D printed nanocomposites; namely PP/Al_2O_3 (0.5 wt%) in Fig. 7a and b, PP/Al_2O_3 (2.0 wt%) in Fig. 7c and d, and PP/Al_2O_3 (4.0 wt%) in Fig. 7e and f, respectively. An excellent interlayer fusion can be observed between the

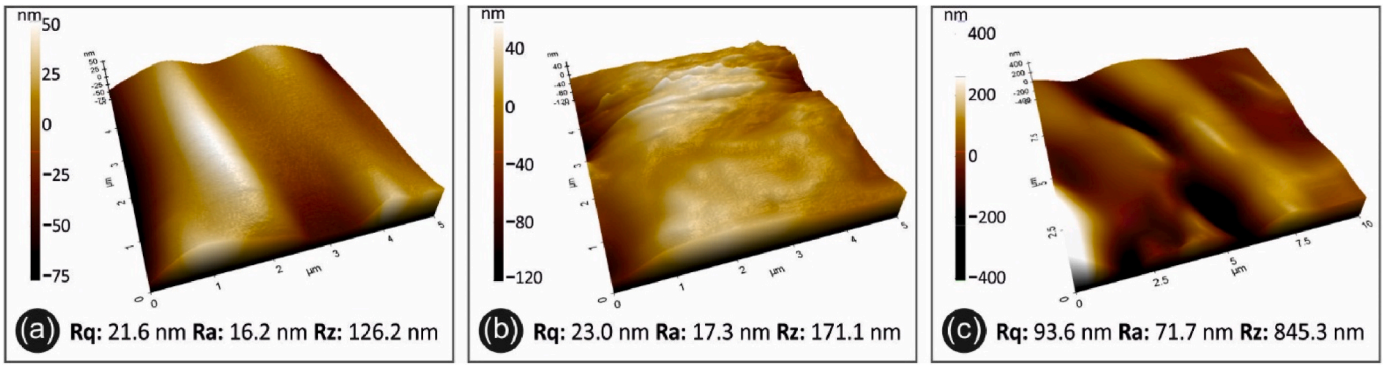

Fig. 8. Three-dimensional (3D) AFM height images together with the corresponding roughness values (given as incest) for: (a) PP/Al_2O_3 (0.5 wt%), (b) PP/Al_2O_3 (2.0 wt%), and (c) PP/Al_2O_3 (4.0 wt%) extruded nanocomposite filaments.

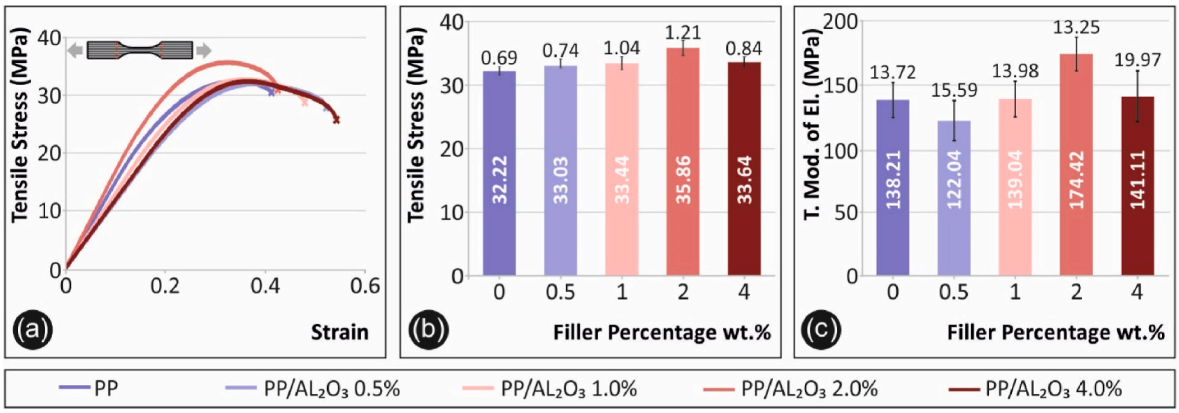

Fig. 9. (a) Tensile stress (MPa) vs strain (%) representative curves for neat PP and PP/Al_2O_3 nanocomposites. (b) Average tensile strength, and (c) average tensile modulus of elasticity values along with the calculated standard deviation values, both as a function of Al_2O_3 different filler loadings (wt.%).

additively deposited layers in all cases, which most likely could result in high interfacial shear strength of the layers and the filaments of the bulk parts. As such, this could drive into high mechanical performance 3D printed nanocomposite parts with a potential enhancement and reinforcement of their mechanical properties due to the presence of Al_2O_3 nanofillers. The high quality of interlayer fusion indirectly proves i) the optimum 3D printing parameters employed in this study, as well as ii) plausibly homogeneously dispersed alumina nanofillers in the PP produced filaments, since nanoparticle aggregation in the utilized filament as feedstock could significantly affect the 3D printing quality introducing inhomogenities, defects, discontinuities, etc. It is well-known that the existence of micro-aggregates in the filament feedstock could impart structural defects in the final 3D printed samples, since it can cause nozzle clogging and thus affect the polymer melt rheological properties. In the nanocomposites 3D printed herein, it is worth mentioning that only in the case of PP/Al_2O_3 (4.0 wt%) nanocomposite the SEM side surface microstructure reveals some inhomogenity in the 3D printed layer thickness, which is most likely, attributed to the increased polymer melt viscosity hampering the 3D printing filamentous extrusion process.

3.4. AFM surface roughness analyses of the extruded nanocomposite filaments

Fig. 8 shows the three-dimensional (3D) AFM images together with the corresponding roughness values (R_q: mean square roughness value, R_a: average roughness value, R_z: maximum roughness value in the "z" direction) for the different PP/Al_2O_3 nanocomposite extruded filaments. The images are representative and have been captured from AFM scans with an area of 5 × 5 μm^2. Apparently, at low filler content (at 0.5 wt%) the nanocomposite filament surface roughness values are relatively low attributed to the PP only polymeric surface (Fig. 8a). On the other hand, the average roughness (R_a) increases to 17.3 nm and 71.7 nm for the PP/Al_2O_3 (2.0 wt%) and PP/Al_2O_3 (4.0 wt%) nanocomposite filaments, respectively. It could be observed that all roughness values, derived from the corresponding nanocomposite filaments surface captured images given as an inset in each sample, are increasing with the increased filler loading. This increase could be attributed to nanoparticles presence onto the filament surface and/or polymer chain conformation i.e. possibly in the form of some crystals' formation induced by the nanoparticle inclusions.

3.5. Tensile properties of 3D printed neat PP and PP/Al_2O_3 nanocomposites

In Fig. 9, the tensile properties of the 3D printed neat PP, as well as PP/Al_2O_3 nanocomposites with 0.5, 1.0, 2.0 and 4.0 wt % filler loadings are depicted. Fig. 9a illustrates the comparative and representative stress-strain curves for the different specimens, while Fig. 9b shows the average tensile strength values and Fig. 9c the tensile modulus of elasticity average values, along with the corresponding standard deviations. As it can be observed, Al_2O_3 NPs have a more prominent reinforcement mechanism with the strength and elastic modulus (stiffness indicator) increasing both at 2.0 wt% filler loadings with very sound increase, while only marginally improved for the 1.0 wt% and 4.0 wt% nanocomposites. Moreover, it can be reported that for all filler loadings, apart from the PP/Al_2O_3 (0.5 wt%) specimens, there has been observed an increase in both the tensile strength and moduli values, indicating an efficient nanoparticle reinforcing mechanism, as well as an achieving high quality interlayer fusion, without interlayer voids, i.e., due to filler agglomerates, etc. that could act further as stress concentration points; points that crack initiation could occur, etc. Specifically, the strength increases by 2.5%, 3.8%, 11.3% and 4.1% for the PP/Al_2O_3 with 0.5, 1.0, 2.0 and 4.0 wt%, respectively. On the other hand, the elastic modulus shows a knock-down effect for the 0.5 wt% nanocomposite (~13.2%), while increasing for all other filler loadings i.e., marginally for the 1.0 wt% (~0.6%) and 4.0 wt% (~2.1%) and significant enhancement for the 2.0 wt% nanocomposite (~26.2%). It can be assumed that the Al_2O_3 NPs induce a mechanical reinforcement mechanism for all the different loadings; however, the 2.0 wt% loading is the optimum getting an increase in both the materials' strength and stiffness with quite promising enhancements as compared to the reference neat PP material. By further increasing the filler loading to 4.0 wt%, specimens clearly reveal a marginal improvement and almost identical mechanical behaviour with the unfilled PP. This is more precisely a proof that at 2.0 wt% already the mechanical percolation threshold has been achieved within the polymer matrix by the Al_2O_3 NPs. Further filler loading increase, i.e., above 4.0 wt% is expected that it will not affect the material's mechanical properties and result in any possible enhancement. Albeit Al_2O_3 NPs and especially due to the nanoparticulate nature, they will probably start to coagulate in the polymer melt, which could have then an adverse property result and a plausible pronounced knock-down effect in the PP mechanical properties. Namely, already for the highest filled system i.e., PP/Al_2O_3 (4.0 wt%), there is not mechanical reinforcement for the tensile strength and modulus due to possible micro-aggregates formation and disturbed optimum nanoparticles dispersion that could result in polymer melt inhomogeneous rheology that could negatively influence the 3D printing process, which also could affect further a 3D printed object layer thickness variation, etc. manifested by the corresponding SEM side surface investigations.

Relatively, there are several possible mechanisms that might lead to an increase in the polymeric materials' strength and stiffness, i.e. the high quality of nanoparticle dispersion in the polymer matrix [42], the optimum polymer melt rheology and temperature during melt

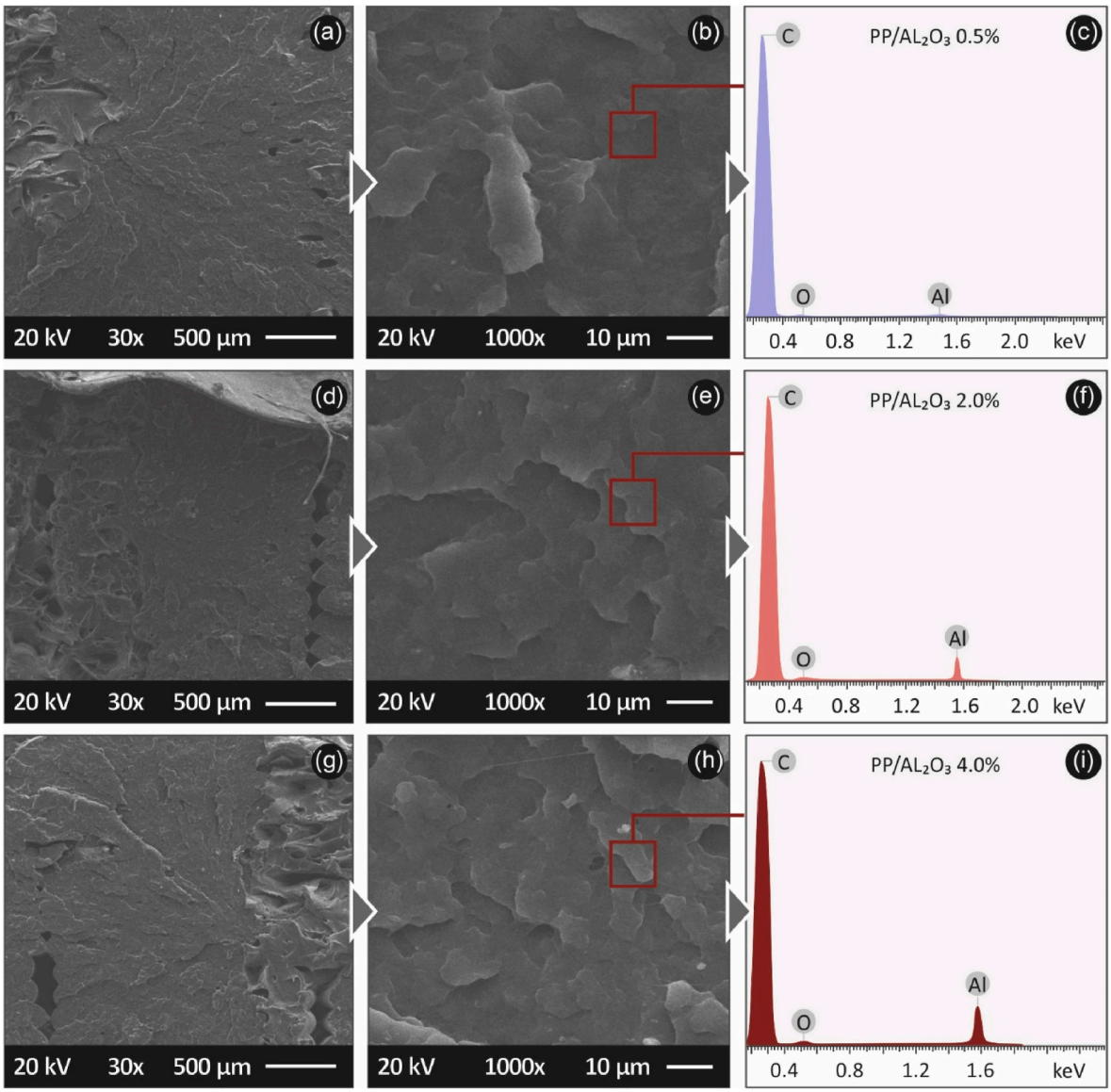

Fig. 10. Fractured surface morphology of 3D printed PP/Al_2O_3 nanocomposites at two different magnifications: (a, b) PP/Al_2O_3 (0.5 wt%), (c, d) PP/Al_2O_3 (2.0 wt %), and (e, f) PP/Al_2O_3 (4.0 wt%).

processing [43,44], and the interaction of nanoparticle inclusions with the polymer matrix [27], amongst others. The effective size and geometry of the filler holds also an important role in determining the mechanical properties of the final composites [45]. To that end, there is a general rule that as the size of the filler particles decrease, the effective filler surface area increases along with the interactions with the polymer matrix. Moreover, it should be always considered that at higher filler loadings the polymer chains become immobilized, while there is a possibility of significant stress concentration upon plausible nanoparticle agglomeration [41]. This may result into potential fracture points and/or points that the fracture process could initiate and thus degrading overall the mechanical performance of the investigated nanocomposites [46].

3.6. SEM/EDS fractography investigations of the tensile test specimen fractured surfaces

Fig. 10 depicts the fractography microstructural investigations of FFF 3D printed PP/Al_2O_3 nanocomposites after the tensile test experiments, indicating both the specimens fracture characteristics, as well as highlighting the printed sample's internal microstructure i.e., existence of voids, extent of the adjacent filament fusion, etc. More specifically, PP/Al_2O_3 (0.5 wt%) (Fig. 10a and b) compared to PP/Al_2O_3 (2.0 wt%) (Fig. 10d and e), and PP/Al_2O_3 (4.0 wt%) (Fig. 10g and h) fractured surfaces are shown at two different magnifications to elucidate the different underlying fracture mechanisms. For all PP/Al_2O_3 nanocomposites, both the low and the high magnification images, show relatively similar characteristics i.e., quite rough surfaces, representing thus a pronounced "ductile" fracture mechanism with polymeric regions/fracture spikes exhibiting a typical morphology of an amorphous polymeric material. The rough fractured surfaces are due to the mechanical energy being efficiently stored elastically by the samples' macromolecular chains and/or the Al_2O_3 NP inclusions, with the most prominent reinforcement mechanism found for the 2.0 wt% nanocomposite as discussed in the previous section. Another important point to be mentioned, observed mainly at the low magnification images (Fig. 10a, d and 10g) of the PP/Al_2O_3 nanocomposite fractured surfaces is that some micro voids could be seen for the 2.0 and 4.0 wt% filler loading in the internal structure of the 3D printed samples between the filaments. This is due to the worse filament fusion with the increased NP

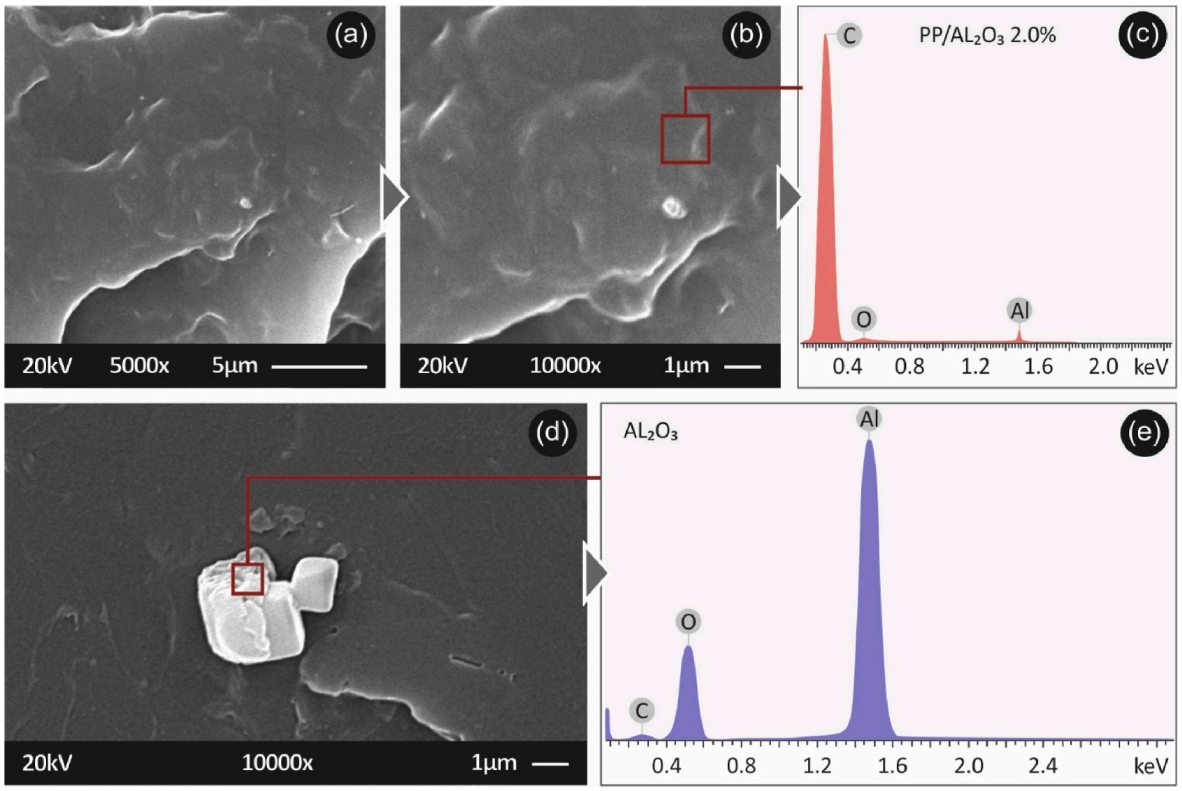

Fig. 11. Fractured surface morphology of 3D printed PP/Al_2O_3 2.0 wt% nanocomposites at high magnifications: (a) 5000x, (b) 10000x. (d) overall, minimum number of filler agglomerations were observed, while the corresponding EDS graphs verify this argument, with Al existence: (c) being low in most cases and (e) dominates the graph in the agglomeration.

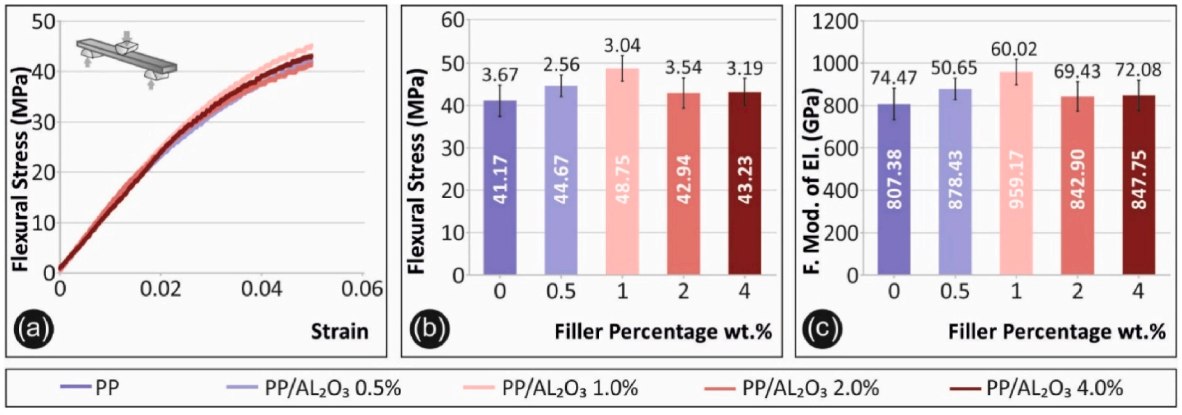

Fig. 12. (a) Flexural stress (MPa) vs strain (%) representative curves for neat PP and PP/Al_2O_3 nanocomposites. (b) Flexural strength, and (c) flexural modulus of elasticity average values, along with the calculated standard deviation values, both as a function of Al_2O_3 different filler loadings (wt.%).

loading in the PP matrix, being in good agreement with the SEM side surface microstructural analyses and the interpretations for MVR presented in the previous sections.

Additionally, in Fig. 10 the corresponding EDS analysis for each filler loading is shown (Fig. 10e, f, 10i), with the existence of Al in all cases verifying the material in the nanocomposites at low concentrations, indicating a good filler dispersion in the polymer matrix.

The single screw extruder used in this work has a special screw with geometry designed to achieve satisfactory mixing results for the materials and the (nano)additives, according to its vendor. Additionally, matrix material was milled in powder form, instead of its original pellets form. It was mixed at high shear conditions for a long period of time with the filler nano powder, to contribute to the increase of the filler dispersion in the polymer matrix. High magnification images indicated typical ductile polymer fracture and good filler dispersion (Fig. 11a and b), with the corresponding EDS graph (Fig. 11c) verifying the low Al concentration in the observed area. Minimum agglomerations were observed (Fig. 11d) and, as expected, Al dominates the graph in the corresponding EDS analysis of the specific specimen's region (Fig. 11e).

3.7. *Flexural properties of 3D printed neat PP and PP/Al_2O_3 nanocomposites*

In Fig. 12, the flexural properties of 3D printed neat PP and PP/Al_2O_3 nanocomposite specimens with 0.5, 1.0, 2.0 and 4.0 wt % filler loadings are depicted. Fig. 12a shows representative flexural stress-strain curves for different tested samples. Fig. 12b illustrates the average flexural strength response, while Fig. 12c, illustrates the average flexural

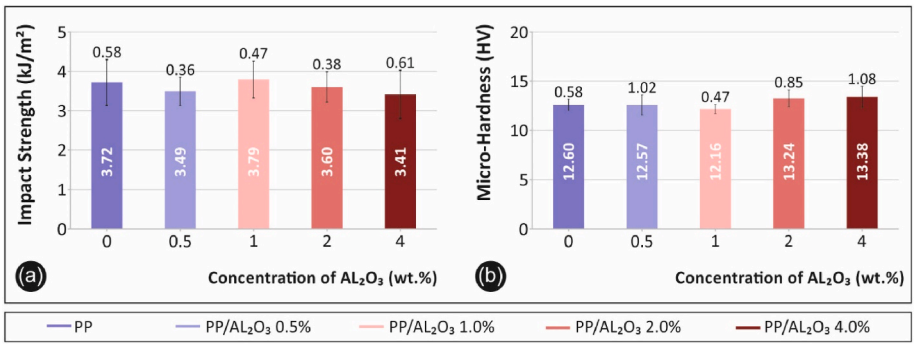

Fig. 13. (a) Charpy's notched impact test results (kJ/m^2), and (b) Micro-hardness (Vickers (HV)) performance of the neat PP compared to the PP/Al_2O_3 nanocomposites (both properties are shown as the calculated mean values together with the corresponding standard deviation).

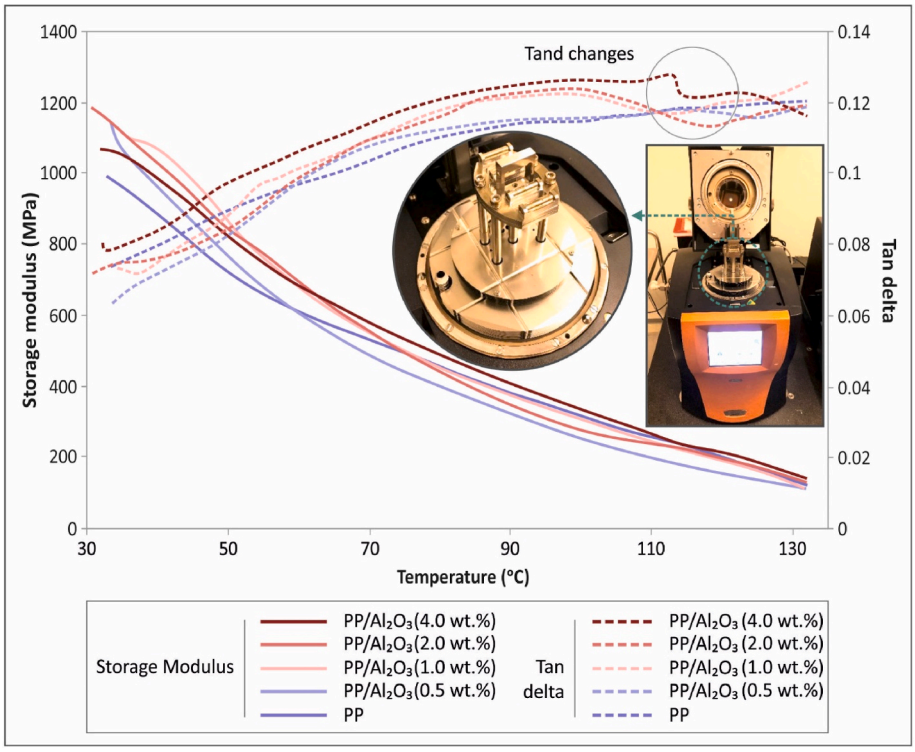

Fig. 14. Storage modulus and Tan delta plots of the neat PP and PP/Al_2O_3 nanocomposites at different filler loadings.

modulus of elasticity of the 3D printed specimens. In all cases, the mean values along with the calculated standard deviations are presented. In contrast to the tensile mechanical properties, alumina nanoparticulate inclusions induced a pronounced reinforcing mechanism in the flexural strength and stiffness of the nanocomposites at all filler loadings. Especially, the flexural strength increases by approximately 8.5%, 18.4%, 4.3% and 4.8% for the 0.5 wt%, 1.0 wt%, 2.0 wt% and 4.0 wt% PP/Al_2O_3 nanocomposites, respectively. On the other hand, the flexural modulus increases by 8.8%, 18.9%, 4.3% and 5.1% for the 0.5, 1.0, 2.0 and 4.0 wt% filler loadings, respectively. The most compelling finding is that PP/Al_2O_3 (0.5 wt%) nanocomposite maintained increased flexural modulus, which is an opposite behaviour compared to the tensile response, where a knock-down effect has been experimentally observed. Overall, the best performance in terms of flexural properties of the PP/Al_2O_3 nanocomposites has been obtained for the 1.0 wt% filler loading with an apparent and clear reinforcing mechanism by ~18.5% in both the flexural modulus and strength values.

3.8. *Impact properties and micro-hardness of 3D printed neat PP and PP/Al_2O_3 nanocomposites*

Fig. 13a shows the average values of the Charpy's notched impact test results for neat PP and PP/Al_2O_3 nanocomposites at different filler loadings (kJ/m^2). Fig. 13b presents the respective micro-hardness (Vickers (HV)) response of the neat PP and PP/Al_2O_3 nanocomposites. Specifically, in Fig. 13a, impact strength mean values are presented for the different 3D printed specimens. As it can be observed, the impact strength is marginally enhanced by the presence of alumina NPs in the polymer matrix only in the case of 1.0 wt% filler loading, while for all the other filler loadings there is a very slight decrease (almost negligible). The slight decrease in the impact strength may be attributed to i) some induced interlayer voids in the samples' bulk and internal structure with the increased nanoparticle loading, discussed in more detail in the SEM fractography analyses section, as well as ii) a possible hampered polymer chain interdiffusion between the different layers and the adjacent filaments during melt deposition, due to the increase of the melt viscosity with the increased particle filler loading, accompanied

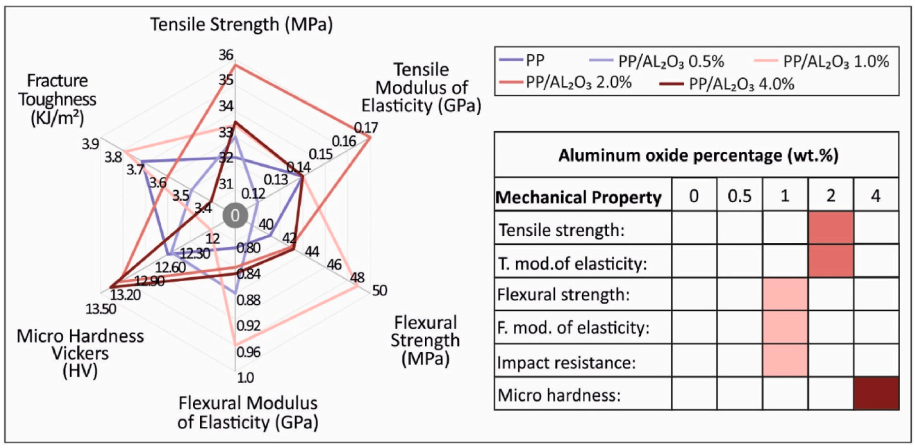

Fig. 15. Overall results on the mechanical properties and performance of neat PP and PP/Al_2O_3 3D printed nanocomposites.

with hindered polymer chain mobility. Regarding the micro-hardness (Fig. 13b), PP/Al_2O_3 nanocomposites at 0.5 wt% and 1.0 wt% exhibited almost identical behavior with the neat PP, while at 2.0 wt% and 4.0 wt% a marginal improvement has been observed. The enhancement in the microhardness values is directly associated with the stiffening of the material induced by the alumina nanoparticles in the PP polymer matrix.

3.9. Thermomechanical analysis of 3D printed neat PP and PP/Al_2O_3 nanocomposites

Fig. 14 illustrates the response of storage modulus and Tand, as a function of temperature, derived from the DMA thermomechanical experiments, for all studied material cases. Storage modulus at low temperatures (~30 °C) coincides with the flexural modulus of the tested material. Furthermore, storage modulus reveals a decreasing tendency with the increase in temperature. The highest damping is recorded for the cases of 0.5, 1.0 and 2.0 wt% doped samples, and marginally increased for the 4.0 wt%. On the other hand, tand exhibits an increasing trend up to the temperature range of 90–100 °C, indicating that up to this temperature range the mechanical energy is stored elastically in the polymeric macromolecular chains; however, with a decreased ability as the temperature increases, manifested by the decreased storage moduli values. On the other hand, >100 °C the tand values show a drop revealing the softening of the material before fusion, and the transition to the viscoelastic regime.

4. Conclusions

In this work, novel nanocomposite filaments of PP/Al_2O_3 were developed in various concentrations, from 0.5 wt% to 4 wt%. Next, the developed filaments were utilized to fabricate standard samples using Fused Filament Fabrication (FFF). To assess the response of the developed structures to nano-filler loading, the 3D printed samples were comprehensively characterized employing mechanical, viscoelastic, physicochemical and fractographic analyses. In specific, mechanical testing (tension, flexure, impact), micro-hardness testing, Raman spectroscopy, Atomic Force Microscopy, Dynamic Mechanical Analysis, Scanning Electron Microscopy and Melt flow testing, were employed. The following conclusions can be derived:

Quasi-static mechanical performance improved in general with the incorporation of alumina nanoparticles, with evidence that 2.0 wt % filler loading, provided overall the highest improvement among others.

On the contrary to tensile and flexure, impact strength reached maximum values at filler loading 1.0 wt%, whilst micro-hardness value, at even higher filler loading, i.e., 2.0 and 4.0 wt%. This finding may also be linked to the increase of viscosity, due to the introduction of the nanofillers, which was manifested by Melt Flow testing.

Raman spectroscopy verified the polymer structure and the incorporated Al_2O_3 NPs in the polymer matrix. Raman spectra were very sensitive to filler loading increase, starting from 0.5 wt%, which is an indication of homogenously dispersed nanofillers in the polymer matrix. Atomic force microscopy of the extruded filaments revealed the introduction of roughness at the nanoscale, induced by the Al_2O_3 NPs.

Al_2O_3 NPs generally increased the viscosity of the polymer melt at all filler loadings; however, all nanocomposites were found to be within the viscosity range allowing for an efficient filamentous FFF extrusion printing process.

Scanning Electron Microscopy micrographs of the 'as-printed' samples, exhibited exceptional interlayer fusion, which improves interlayer adhesion and leads to performance increase. The resultant interlayer fusion confirms both the importance of appropriately set printing parameters and could be indicative of homogeneously dispersed alumina nanoparticles in the thermoplastic matrix, as the opposite may lead to defects, discontinuities, etc. that are detrimental to the final quality. On the other hand, micrographs of the fracture surfaces, confirmed the mechanical performance response in tension, revealing in general a ductile failure at low and high filler loadings, respectively.

Dynamic mechanical analysis confirmed the stiffening mechanism recorded by mechanical testing. A softening effect at high temperatures (>100 °C) for the neat PP and PP/Al_2O_3 nanocomposite was revealed.

As a summary, the overall mechanical response of the 3D printed nanocomposites investigated in this study are illustrated in the histogram of Fig. 15. As it is shown, the introduction of the nanoparticles in the polymer matrix improves the mechanical properties of the pure polymer material for concentrations up to 2 wt, with the highest improvement developed in the 2.0 wt % for the tensile and 1.0 wt for the flexural properties. For higher concentrations, the nanocomposite exhibited a marginal improvement in the mechanical properties. It can be concluded that commercially available polypropylene reinforced with Al_2O_3 nanoparticles, maybe a useful solution for demanding applications, benefiting the engineering thermoplastics industry.

Author statement

The paper has been initially submitted to your journal on the May 8, 2021, and we received it back on the 17th of November with some major revisions to be considered.

In the revised version of the manuscript as well as in the response to reviewer comments submitted document, we explain point-by-point the details of the major-revisions in the manuscript (using the "track-changes" MS function in the re-submitted version of the manuscript) and our responses to the reviewer's comments.

We believe that the paper is at the forefront of research for **FFF 3D**

printed polymeric nanocomposites, utilising a widely used and commercially available thermoplastic engineered polymer and low-cost inorganic nanoparticles. Moreover, for the nanocomposite extruded filament materials, as well as the 3D printed nanocomposites has been elucidated all the plausible underlying mechanisms for the mechanical reinforcement and the material interaction mechanisms at different scales (nano-/micro-/macro).

Also, this work is of benefit for the polymer and plastics industry, as it demonstrates that commercially available PP reinforced with Al_2O_3 NPs, maybe a solution for applications requiring enhanced material's static mechanical, impact and dynamic thermomechanical properties.

All in all, we are convinced that the submitted paper is suitable for publication in **Polymer Testing** Journal, due to main the manuscript's focus i.e. to deliver a clear message and understanding of the **"polymer material's design"** approach to yield an optimum "structure-property" relationship of the 3D printed/manufactured nanocomposite specimens.

We would like to thank the reviewers for all the important and critical comments improving the quality of our paper.

On behalf of all my co-authors, I would like to thank you in advance for appreciating our study and hope that the revised version of the manuscript can be accepted for publication. In any other case, we remain at your disposal for any changes or corrections that might be needed.

Declaration of competing interest

The authors declare that they have no known competing financial interests or personal relationships that could have appeared to influence the work reported in this paper.

Acknowledgments

LT would like to thank the Bodossaki Foundation for financial support in the framework of institutional scholarships. Authors would like to thank Ms. Aleka Manousaki from Institute of Electronic Structure and Laser (IESL), Foundation for Research and Technology (FORTH) Hellas for taking the SEM images presented in this work.

References

[1] V. Shanmugam, D.J.J. Rajendran, K. Babu, S. Rajendran, A. Veerasimman, U. Marimuthu, S. Singh, O. Das, R.E. Neisiany, M.S. Hedenqvist, F. Berto, S. Ramakrishna, The mechanical testing and performance analysis of polymer-fibre composites prepared through the additive manufacturing, Polym. Test. 93 (2021) 106925.

[2] J. Zhang, J. Wang, S. Dong, X. Yu, B. Han, A review of the current progress and application of 3D printed concrete, Compos. Appl. Sci. Manuf. 125 (2019) 105533.

[3] C. Kapnopoulos, E.D. Mekeridis, L. Tzounis, C. Polyzoidis, A. Zachariadis, S. Tsimikli, C. Gravalidis, A. Laskarakis, N. Vouroutzis, S. Logothetidis, Fully gravure printed organic photovoltaic modules: a straightforward process with a high potential for large scale production, Sol. Energy Mater. Sol. Cell. 144 (2016) 724–731.

[4] L. Tzounis, P.I. Bangeas, A. Exadaktylos, M. Petousis, N. Vidakis, Three-dimensional printed polylactic acid (PLA) surgical retractors with sonochemically immobilized silver nanoparticles: the next generation of low-cost antimicrobial surgery equipment, Nanomaterials 10 (2020) 985.

[5] F. Alam, K.M. Varadarajan, S. Kumar, 3D printed polylactic acid nanocomposite scaffolds for tissue engineering applications, Polym. Test. 81 (2020) 106203.

[6] K. Gnanasekaran, T. Heijmans, S. van Bennekom, H. Woldhuis, S. Wijnia, G. de With, H. Friedrich, 3D printing of CNT- and graphene-based conductive polymer nanocomposites by fused deposition modeling, Appl. Mater. Today 9 (2017) 21–28.

[7] K. Takagishi, S. Umezu, Development of the improving process for the 3D printed structure, Sci. Rep. 7 (2017) 39852.

[8] S. Garzon-Hernandez, D. Garcia-Gonzalez, A. Jérusalem, A. Arias, Design of FDM 3D printed polymers: an experimental-modelling methodology for the prediction of mechanical properties, Mater. Des. 188 (2020) 108414.

[9] R. Velu, F. Raspall, S. Singamneni, Chapter 8 - 3D printing technologies and composite materials for structural applications, in: G. Koronis, A. Silva (Eds.), Green Composites for Automotive Applications, Woodhead Publishing, 2019, pp. 171–196.

[10] T.D. Ngo, A. Kashani, G. Imbalzano, K.T.Q. Nguyen, D. Hui, Additive manufacturing (3D printing): a review of materials, methods, applications and challenges, Compos. B Eng. 143 (2018) 172–196.

[11] X. Tian, T. Liu, C. Yang, Q. Wang, D. Li, Interface and performance of 3D printed continuous carbon fiber reinforced PLA composites, Compos. Appl. Sci. Manuf. 88 (2016) 198–205.

[12] N. Vidakis, M. Petousis, L. Tzounis, A. Maniadi, E. Velidakis, N. Mountakis, J. D. Kechagias, Sustainable additive manufacturing: mechanical response of polyamide 12 over multiple recycling processes, Materials 14 (2021) 466.

[13] K. Savvakis, M. Petousis, A. Vairis, N. Vidakis, A.T. Bikmeyev, Experimental determination of the tensile strength of fused deposition modeling parts, in: ASME 2014 International Mechanical Engineering Congress and Exposition, 2014.

[14] N. Vidakis, M. Petousis, A. Vairis, K. Savvakis, A. Maniadi, On the compressive behavior of an FDM Steward Platform part, J. Comput. Des. Eng. 4 (2017) 339–346.

[15] N. Vidakis, M. Petousis, A. Vairis, K. Savvakis, A. Maniadi, A parametric determination of bending and Charpy's impact strength of ABS and ABS-plus fused deposition modeling specimens, Progr. Add. Manufact. 4 (2019) 323–330.

[16] N. Vidakis, M. Petousis, K. Savvakis, A. Maniadi, E. Koudoumas, A comprehensive investigation of the mechanical behavior and the dielectrics of pure polylactic acid (PLA) and PLA with graphene (GnP) in fused deposition modeling (FDM), Int. J. Plast. Technol. 23 (2019) 195–206.

[17] J.M. Chacón, M.A. Caminero, E. García-Plaza, P.J. Núñez, Additive manufacturing of PLA structures using fused deposition modelling: effect of process parameters on mechanical properties and their optimal selection, Mater. Des. 124 (2017) 143–157.

[18] N. Vidakis, A. Maniadi, M. Petousis, M. Vamvakaki, G. Kenanakis, E. Koudoumas, Mechanical and electrical properties investigation of 3D-printed acrylonitrile–butadiene–styrene graphene and carbon nanocomposites, J. Mater. Eng. Perform. 29 (2020) 1909–1918.

[19] L. Tzounis, M. Petousis, S. Grammatikos, N. Vidakis, 3D printed thermoelectric polyurethane/multiwalled carbon nanotube nanocomposites: a novel approach towards the fabrication of flexible and stretchable organic thermoelectrics, Materials 13 (2020) 2879.

[20] A.P. Taylor, C.V. Cuervo, D.P. Arnold, L.F. Velásquez-García, Fully 3D-printed, monolithic, mini magnetic actuators for low-cost, compact systems, J. Microelectromech. Sys. 28 (2019) 481–493.

[21] C.J. Hohimer, G. Petrossian, A. Ameli, C. Mo, P. Pötschke, 3D printed conductive thermoplastic polyurethane/carbon nanotube composites for capacitive and piezoresistive sensing in soft pneumatic actuators, Add. Manufact. 34 (2020) 101281.

[22] T. Le, B. Song, Q. Liu, R.A. Bahr, S. Moscato, C. Wong, M.M. Tentzeris, A novel strain sensor based on 3D printing technology and 3D antenna design, in: 2015 IEEE 65th Electronic Components and Technology Conference (ECTC), 2015, pp. 981–986.

[23] N. Vidakis, M. Petousis, A. Maniadi, E. Koudoumas, M. Liebscher, L. Tzounis, Mechanical properties of 3D-printed acrylonitrile–butadiene–styrene TiO2 and ATO nanocomposites, Polymers 12 (2020) 1589.

[24] N. Vidakis, M. Petousis, E. Velidakis, M. Liebscher, L. Tzounis, Three-dimensional printed antimicrobial objects of polylactic acid (PLA)-Silver nanoparticle nanocomposite filaments produced by an in-situ reduction reactive melt mixing process, Biomimetics 5 (2020) 42.

[25] D. Thaler, N. Aliheidari, A. Ameli, Mechanical, electrical, and piezoresistivity behaviors of additively manufactured acrylonitrile butadiene styrene/carbon nanotube nanocomposites, Smart Mater. Struct. 28 (2019), 084004.

[26] M. Jin, C. Neuber, H.-W. Schmidt, Tailoring polypropylene for extrusion-based additive manufacturing, Add. Manufact. 33 (2020) 101101.

[27] D.G. Papageorgiou, L. Tzounis, G.Z. Papageorgiou, D.N. Bikiaris, K. Chrissafis, β-nucleated propylene–ethylene random copolymer filled with multi-walled carbon nanotubes: mechanical, thermal and rheological properties, Polymer 55 (2014) 3758–3769.

[28] A.D. Valino, J.R.C. Dizon, A.H. Espera, Q. Chen, J. Messman, R.C. Advincula, Advances in 3D printing of thermoplastic polymer composites and nanocomposites, Prog. Polym. Sci. 98 (2019) 101162.

[29] J. Wang, Y. Kazemi, S. Wang, M. Hamidinejad, M.B. Mahmud, P. Pötschke, C. B. Park, Enhancing the electrical conductivity of PP/CNT nanocomposites through crystal-induced volume exclusion effect with a slow cooling rate, Compos. B Eng. 183 (2020) 107663.

[30] L.T. Truong, Å. Larsen, B. Holme, F.K. Hansen, J. Roots, Morphology of syndiotactic polypropylene/alumina nanocomposites, Polymer 52 (2011) 1116–1123.

[31] N. Vidakis, M. Petousis, L. Tzounis, A. Maniadi, E. Velidakis, N. Mountakis, D. Papageorgiou, M. Liebscher, V. Mechtcherine, Sustainable additive manufacturing: mechanical response of polypropylene over multiple recycling processes, Sustainability 13 (2021) 159.

[32] C. Aumnate, S. Limpanart, N. Soatthiyanon, S. Khunton, PP/organoclay nanocomposites for fused filament fabrication (FFF) 3D printing, Express Polym. Lett. 13 (2019) 898–909.

[33] C. Aumnate, P. Potiyaraj, C. Saengow, A.J. Giacomin, Reinforcing polypropylene with graphene-polylactic acid microcapsules for fused-filament fabrication, Mater. Des. 198 (2021) 109329.

[34] Y. Shmueli, Y.-C. Lin, X. Zuo, Y. Guo, S. Lee, G. Freychet, M. Zhernenkov, T. Kim, R. Tannenbaum, G. Marom, D. Gersappe, M.H. Rafailovich, In-situ X-ray scattering study of isotactic polypropylene/graphene nanocomposites under shear during fused deposition modeling 3D printing, Compos. Sci. Technol. 196 (2020) 108227.

[35] L. Lei, Z. Yao, J. Zhou, B. Wei, H. Fan, 3D printing of carbon black/polypropylene composites with excellent microwave absorption performance, Compos. Sci. Technol. 200 (2020) 108479.

[36] S.W. Kwok, K.H.H. Goh, Z.D. Tan, S.T.M. Tan, W.W. Tjiu, J.Y. Soh, Z.J.G. Ng, Y. Z. Chan, H.K. Hui, K.E.J. Goh, Electrically conductive filament for 3D-printed circuits and sensors, Appl. Mater. Today 9 (2017) 167–175.
[37] J. Gangwar, B.K. Gupta, S.K. Tripathi, A.K. Srivastava, Phase dependent thermal and spectroscopic responses of Al2O3 nanostructures with different morphogenesis, Nanoscale 7 (2015) 13313–13344.
[38] X. Guo, Z. Lin, Y. Wang, Z. He, M. Wang, G. Jin, In-line monitoring the degradation of polypropylene under multiple extrusions based on Raman spectroscopy, Polymers 11 (2019) 1698.
[39] P. Mukherjee, M. Roy, B.P. Mandal, G.K. Dey, P.K. Mukherjee, J. Ghatak, A. K. Tyagi, S.P. Kale, Green synthesis of highly stabilized nanocrystalline silver particles by a non-pathogenic and agriculturally important fungusT, asperel., Nanotechnol. 19 (2008), 075103.
[40] R.S. Krishnan, Raman spectrum of alumina and the luminescence and absorption spectra of ruby, Nature 160 (1947), 26-26.
[41] L. Tzounis, S. Pegel, N.E. Zafeiropoulos, A. Avgeropoulos, A.S. Paipetis, M. Stamm, Shear alignment of a poly(styrene-butadiene-styrene) triblock copolymer/MWCNT nanocomposite, Polymer 131 (2017) 1–9.
[42] L. Tzounis, M. Hegde, M. Liebscher, T. Dingemans, P. Pötschke, A.S. Paipetis, N. E. Zafeiropoulos, M. Stamm, All-aromatic SWCNT-Polyetherimide nanocomposites for thermal energy harvesting applications, Compos. Sci. Technol. 156 (2018) 158–165.
[43] L. Tzounis, T. Gärtner, M. Liebscher, P. Pötschke, M. Stamm, B. Voit, G. Heinrich, Influence of a cyclic butylene terephthalate oligomer on the processability and thermoelectric properties of polycarbonate/MWCNT nanocomposites, Polymer 55 (2014) 5381–5388.
[44] M. Liebscher, L. Tzounis, P. Pötschke, G. Heinrich, Influence of the viscosity ratio in PC/SAN blends filled with MWCNTs on the morphological, electrical, and melt rheological properties, Polymer 54 (2013) 6801–6808.
[45] L. Tzounis, S. Debnath, S. Rooj, D. Fischer, E. Mäder, A. Das, M. Stamm, G. Heinrich, High performance natural rubber composites with a hierarchical reinforcement structure of carbon nanotube modified natural fibers, Mater. Des. 58 (2014) 1–11.
[46] N. Vidakis, M. Petousis, E. Velidakis, M. Liebscher, V. Mechtcherine, L. Tzounis, On the strain rate sensitivity of fused filament fabrication (FFF) processed PLA, ABS, PETG, PA6, and PP thermoplastic polymers, Polymers 12 (2020) 2924.